HiSST: 3rd International Conference on
High-Speed Vehicle Science Technology
14 -19 April 2024, Busan, Korea

The dynamic test of the longitudinal stage separation for the parallel-staged two-stage-to-orbit vehicle in shock tunnel

Yue Wang[1], Yunpeng Wang[2]

Abstract

Parallel-staged two-stage-to-orbiter (TSTO) vehicle is one of the promising next-generation reusable launch vehicles and comprises the booster and the orbiter. However, the TSTO hypersonic stage separation introduces strong shock waves and results in complex aerodynamic interaction into the interstage flowfield, which increases the risk of the stage separation and would determine the success of the launch mission. Thus, the longitudinal stage separation (LSS) is proposed, in which the orbiter accelerates along the upper surface of the booster with the unnoticeable interstage gap, so the strong shock-shock interaction (SSI) might be absent in the interstage flowfield. The dynamic tests of the TSTO stage separation are conducted in the JF-12 hypersonic flight condition duplicated shock tunnel at Mach 7. The TSTO vehicle comprises the wave-rider and the spaceplane as the booster and the orbiter. The dynamic test methodology of the multi-body vehicle stage separation in the short effective test time ground facility is clarified, including the high-speed pneumatic ejection to launch vehicle model system (HPELS) to make the LSS and high-speed Schlieren visualization and image processing techniques to capture the separation trajectory. Besides, the unsteady shock wave structure and wall pressure are also observed and examined. The LSS of the TSTO vehicle in the JF-12 shock tunnel is examined at angles of attack (AoA) of 8.3 and 4.5 deg. The results show that the small interstage gap of LSS leads to weak type I and VI SSI, with short-duration weak shock reflections at a high AoA. Furthermore, no shock reflection is observed at a small AoA. Additionally, no stage re-contact is observed, and the safety and feasibility of the LSS principle for the parallel-staged TSTO vehicle are demonstrated.

Keywords: *Reusable launch vehicle, stage separation, hypersonic, aerodynamic interaction, test*

Nomenclature

p – Pressure
T – Temperature
Ma – Mach number
Re – Reynolds number
q – Dynamic pressure
AoA – Angle of attack
v – Vehicle speed
U – Flow speed
Subscripts
0 – Total condition
∞ – Freestrem condition

1. Introduction

Two-body configurations are common in aeronautics and astronautics, in which high-speed flows over two-body are inherently complex and important. The parallel-staged two-stage-to-orbit (TSTO) vehicle as a typical two-body configuration is composed of a booster with combined air-breathing propulsion and an orbiter with a rocket engine vehicle. Moreover, the stage separation typically happens in the hypersonic condition, i.e., around Mach 7, so the high-speed flow past a TSTO vehicle such that a two-body system probably includes shock wave-shock wave interaction (SSI) and shock wave-boundary

[1] *Institute of Mechanics, Chinese Academy of Sciences, No. 15 Beisihuan Western Road, Beijing, China, wangyue@imech.ac.cn*
[2] *Institute of Mechanics, Chinese Academy of Sciences, No. 15 Beisihuan Western Road, Beijing, China, wangyunpeng@imech.ac.cn*

layer interaction (SBLI) as well as flow separation [1] That unsteady flow involves complex aerodynamic interference and multi-body movements causing the TSTO stage separation to be challenging and determining the safety of the stage separation even a TSTO mission or not.

The separation scheme determines the effect of the stage separation [2]. Most studies concern the analysis of transverse stage separation for TSTO. The orbiter is released and separated toward the normal direction of the booster. Moelyadi et al. [3] performed time-dependent simulations of stage separation considering the effects of unsteady flows since the orbiter's harmonic motions. The results showed that the unsteady effects must be carefully treated when the orbiter's aerodynamics have a strong change. Bordelon et al. [4] conducted the wind tunnel test to examine the TSTO stage separation flowfield at Mach 2.74-4.96, the results showed that the shock wave plays a big role in the aerodynamics and the vehicle could be statically instability at some positions during separation. Wang et al. [5] performed dynamic numerical simulations of the transverse stage separation for the TSTO vehicle at Mach 7 and investigated the dynamic stability of the vehicles based on the center of pressure analysis methods. The results showed that the complex dynamic SSI interaction and multi-body movements coupling, and safe stage separation for the TSTO vehicles is difficult because of the narrow safe separation boundary. The strong aerodynamic interference that occurs between stages during separation may be detrimental to the safety separation of TSTO [6]. Thus, Wang et al. [2] proposed a new separation scheme, i.e., longitudinal stage separation (LSS), for parallel-staged TSTO vehicles. The separation of the orbiter along the upper wall of the booster under the thrust of the rocket engine, with tiny or even no gaps, may result in weak aerodynamic interference [7,8]. To continue deeply revealing the aerodynamic interference and flow mechanism of the LSS for parallel-staged TSTO vehicle, the experimental results of the dynamic test in the JF-12 hypersonic flight condition duplicated shock tunnel.

2. TSTO model

The parallel-staged TSTO model for the dynamic LSS test consists of a wave-rider and a spaceplane as the booster and the orbiter respectively. The detailed TSTO concept and related works can be depicted in those studies. Figure 1 presents the tested TSTO model size. The length of the booster is l_b = 1 m, and its center of gravity (CG) is located at (0.738, -0.05, 0) m. The length of the orbiter is l_o = 0.4 m, and its CG is located at (0.740, 0.016, 0) m. Figure 2 shows the photo of the tested TSTO model in the JF-12 shock tunnel test section and associated devices for the dynamic stage separation. The AoA of the TSTO vehicle is defined as the relative angle between the airflow and the booter's upper surface. In the testing, the AoA is adjusted by the angle between the model strut and the pedestal in the test section. As shown in Fig. 2, in the testing, the booster is equipped on the model strut. Additionally, the orbiter moves along the booster's upper surface with enough high impulse, in which, high-pressure nitrogen pushes the cylinder to do work and transfers the impulse to the orbiter by the impact bar. Thus, the dynamic test of LSS is carried out in that way in the JF-12 shock tunnel. The TSTO model is mainly made from aluminum alloy materials. For the CFD simulations and testing, the non-dimensional mass of the orbiter is $m_o/\rho_\infty l_o^3$ = 3175, and the moments of inertia are $I_{xx} / \rho_\infty \cdot l_o^5$ = 21, $I_{yy} / \rho_\infty \cdot l_o^5$ = 210, and $I_{zz} / \rho_\infty \cdot l_o^5$ = 198, respectively. Herein, ρ_∞ = 0.0062 kg·m^{-3} refers to the density of freestream. The mass characteristics of the orbiter model are assessed by computer-aided engineering (CAE) software.

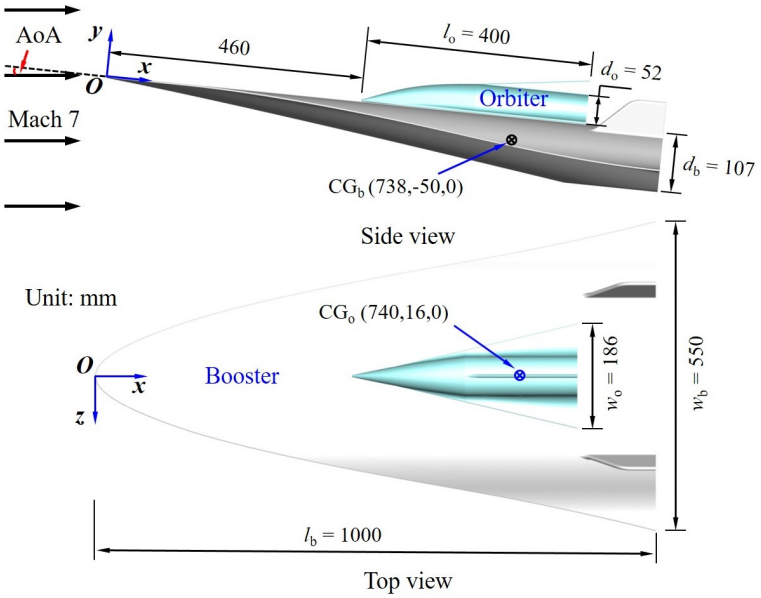

Fig 1. The overall size of the scaled TSTO model

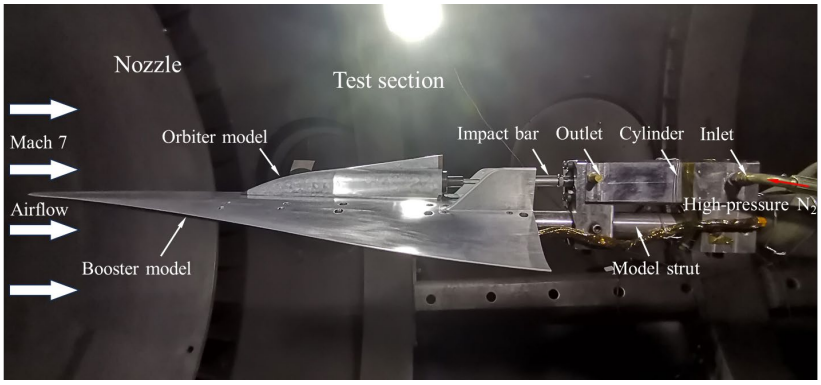

Fig 2. The tested TSTO model in the test section

3. Experimental program

3.1. Test facility and conditions

The experiment was conducted in the JF-12 shock tunnel. The photo of the JF-12 shock tunnel is showed in Fig 3. The JF-12 is the long-test-duration hypersonic detonation-driven shock tunnel that is developed based on the backward-running detonation driver with several innovative techniques [9,10]. JF-12 shock tunnel consists of a damping section, a detonation chamber, a shock tube, a nozzle, and a test section. JF-12 can reproduce the pure airflow with Mach 5 ~ 9 at an altitude of 25-50 km with at least 100 ms effective test time. Figure 3 presents the photo of the JF-12 shock tunnel. The nozzle with a diameter of 2.5 m was employed to generate a nominal Mach 7 hypersonic airflow. Table 1 presents the freestream condition and the angles of attack (AoA) of the TSTO model.

Fig 3. The JF-12 shock tunnel

Table 1. Test condition

p_0, MPa	T_0, MPa	Ma_∞	Re_∞, m^{-1}	q_∞, Pa	AoA, deg
2.63	2393	6.99	8.57×10^5	15444	8.3
2.53	2371	6.95	8.55×10^5	15351	4.5

3.2. Test methodology

In the test, a series of methods for the LSS in the shock tunnel were applied, including a high-speed visualization system (Schlieren and camera), wall pressure distribution, and separation trajectory capturing of the orbiter. Figure 4 shows the schematic of the visualization system, consisting of the Schlieren camera I and the high-speed camera II. Several light-emitting diodes (LEDs) were equipped on the orbiter to be identified clearly by the image trajectory recognition methods. Then the separation motion of the orbiter could be acquired. The pressure on the centerline of the booster wall was measured by the pressure transducer with a range of 50 kPa and an accuracy of 0.25% F.S. (Full scale). The sampling rate is 100 kHz. In addition, a pitot pressure sensor is installed at the exit of the nozzle to measure the airflow conditions. Since the effective test time (100 ~ 130 ms) of the JF-12 shock tunnel is too short to conduct the active dynamic separation for TSTO, the high-speed pneumatic ejection to launch vehicle model system (HPELS) was developed. In the dynamic test, the HPELS applies high impulse on the orbiter and separates from the booster as fast as possible. Figure 2 presents the core components of the HPELS. In the LSS test, the high-pressure nitrogen with around 8 MPa acts as the working fluid to drive the cylinder for imposing the orbiter model a great initial impulse so that the orbiter can separate from the booster within 100 ms. With the appropriate and precise timing control of the HPELS, the orbiter can separate from the booster with an average speed of 8 ~ 13 $m{\cdot}s^{-1}$ in the test. Detailed information on the constitute elements and control of the HPELS was recorded in the previous study [11]. Thus, the LSS could be investigated and measured during the short effective time of the shock tunnel.

The observation window of the JF-12 test section is big enough to capture most of the LSS motion with a diameter of 650 mm as shown in Fig 4. Since the complexity and limitations of the motion data acquired by sensors for moving model, those data are acquired by postprocessing the separation trace results. Several LEDs equipped on the orbiter orientate vertically to the observation window. Therefore, LEDs that show white faculae in the Schlieren video can be identified clearly and easily by the image recognition method (as shown in Fig 5), and then the orbiter's trajectory and pitching angle can be acquired. The non-contact trajectory trace method is cheap, practical, and has minor effects on the dynamic test results because its structure is very lightweight. The detailed information and procedure can be depicted in the work of [12].

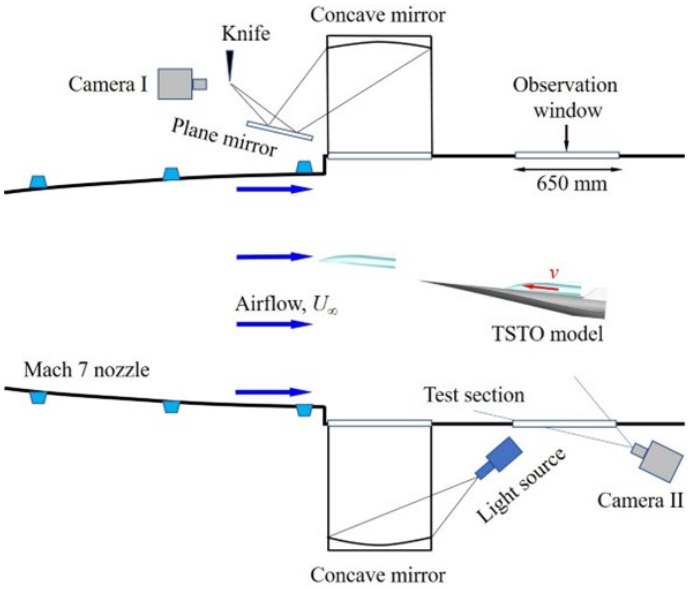

Fig 4. The sketch of the high-speed visualization system in the JF-12 shock tunnel

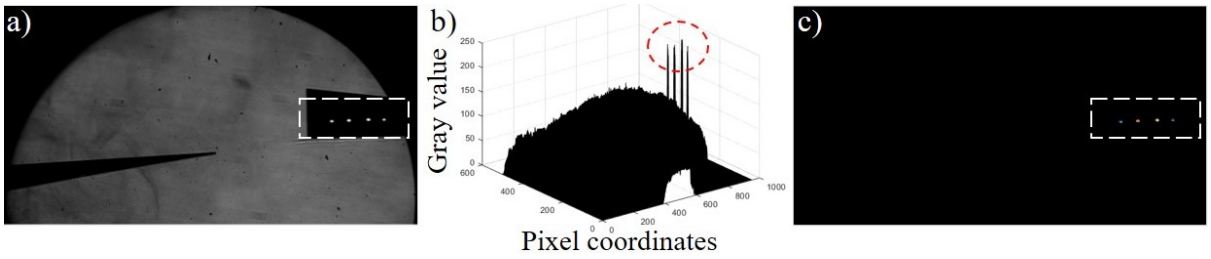

Fig 5. Recognition of LEDs' pixel coordinates on the orbiter model based on the Schlieren image: (a) gray photo of the Schlieren image, (b) the distribution of the gray value, and (c) identification of the LEDs' pixel coordinates.

4. Results and discussion

4.1. Flowfield structure

Figures 6 and 7 present the experimental schlieren photos in some instances during LSS. The flowfields of LSS are governed by the simple type I or VI oblique shock-shock interaction (SSI) and the weak oblique shock reflection in a small gap and weak oblique SBLI after the orbiter separates from the booster. Before instant (d), neither gap nor SBLI occurs between stages. At instant (a), the booster leading edge shock and orbiter shock occur type VI SSI, which turns into a stronger convergent shock directly when the nose of the two stages coincide at instant (b). In addition, the type VI SSI occurs below the booster and affects the lower surface of the booster, as shown in Fig 6c. The orbiter shock sweeps over the lower surface of the booster with a tiny impinge angle, causing a little pressure rise of about 9% compared to the isolated state. Then, the weak shock reflection and weak SBLI are observed as the orbiter is lifted with a gap to the booster by the normal force and nose-up moment. As the orbiter moves away from the booster, SBLI moves downstream along the upper surface of the booster. Finally, the shock reflection disappears, and the only type I SSI remains in the flowfield and an isolated booster. When the TSTS separates at a low AoA condition, i.e., AoA = 4.5 deg, no interstage gap is observed during LSS, let alone the SBLI and shock reflection between stages. Thus, the aerodynamic interaction becomes weaker, two stages separate safer and smoother.

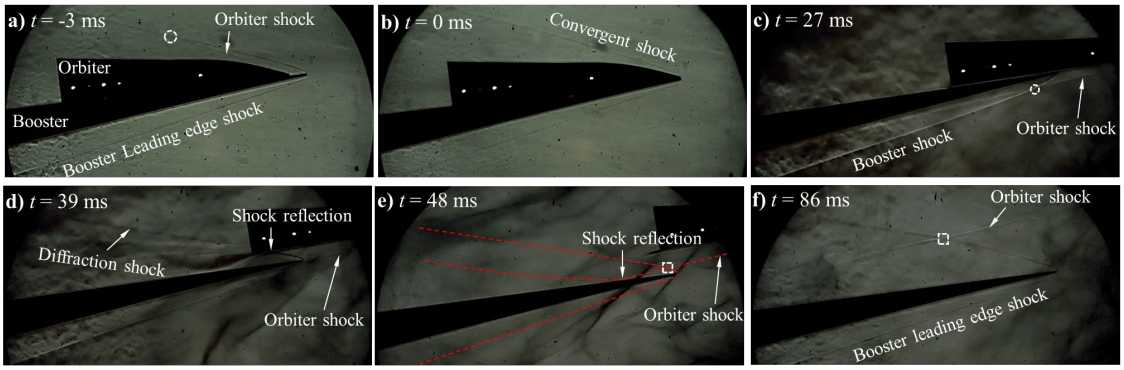

Fig 6. Schlieren photos during LSS at AoA = 8.3 deg

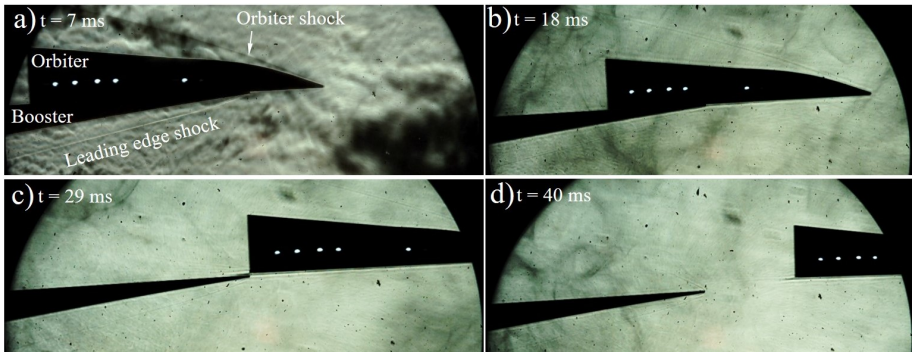

Fig 7. Schlieren photos during LSS at AoA = 4.5 deg

4.2. Wall pressure

Figure 8 and Fig 9 plot the pressure coefficients along the booster's upper wall and lower wall at the AoA = 8.3 deg and 4.5 deg. As shown in Fig 8b, due to the transmitted oblique shock wave from type VI SSI sweeps over the booster's lower wall with a tiny impinge angle, causing a pressure rise about a maximum of 9% compared to the pressure on the undisturbed booster's lower. Moreover, as the impinge location moves upstream along the booster's lower wall with the obiter' separating, the pressure on the forepart ($0.25 < x/l_b < 0.35$) increases while that on the afterbody ($0.40 < x/l_b < 0.45$) decreases, as shown in Fig 8b. As the orbiter is separating from the booster, a shock reflection occurs between two stages which can be observed at instants (e) and (f). Because the shock reflection is weak, it does not induce a high-pressure rise on the booster's upper wall, as shown in Fig 8a. As the separation goes on, the SBLI moves downstream along the booster's upper wall, so the pressure coefficient along the booster's upper wall increases as the shock reflection approaches and decreases.

Due to no shock reflection or SBLI exits between stages, the pressure on the booster is almost unchanged with no apparent pressure rise, as shown in Fig 9. Moreover, as the orbiter separates, the pressure on the booster's upper wall decreases slightly. The pressure on the booster's lower wall also decreases slightly since type VI SSI vanishes. By comparing the pressure response on the booster at two AoA conditions, the aerodynamic interference in the LSS test at AoA = 4.5 deg is weaker than that at AoA = 8.3 deg.

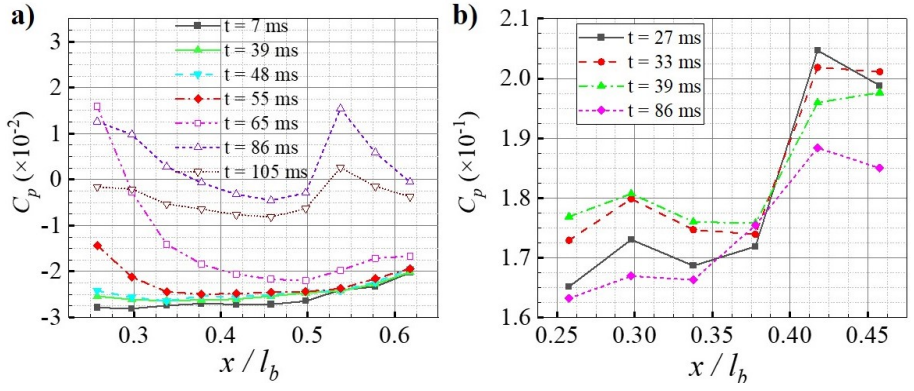

Fig 8. Pressure coefficients on the booster during LSS test at AoA = 8.3 deg: (a) along the upper surface; (b) along the lower surface.

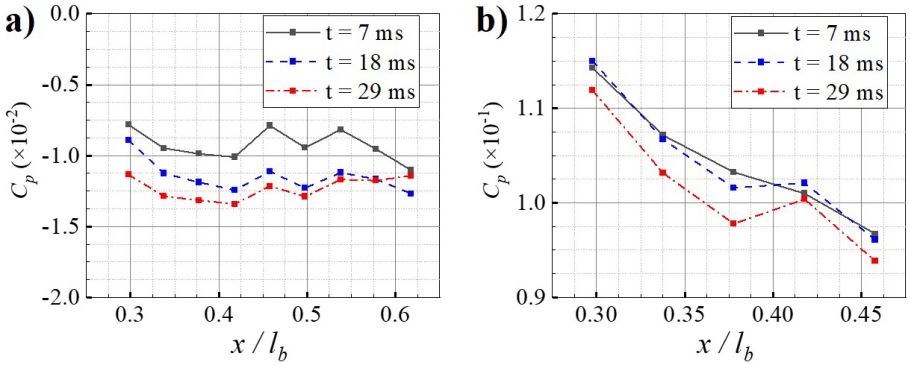

Fig 9. Pressure coefficients on the booster during the LSS test at AoA = 4.5 deg: (a) along the upper surface; (b) along the lower surface.

4.3. Separation trajectory

The non-dimensional orbiter's separation trajectories were captured in the Schlieren video and predicted by the CFD simulation for the LSS at AoA = 8.3 deg and 4.5 deg are illustrated in Fig 10. Additionally, the error bands of the captured results are also shown. In general, the trajectory and pitching angle of the orbiter are consistent in the variation tendency and small disparity between the captured and predicted results for different AoA cases. As shown in Fig 10, the displacements of the CFD and experiment are in good agreement, but the disparity is observed when the orbiter is detaching from the booster ($\triangle$ x/lo $\leqslant$ -1.75) and the orbiter's pitching angle varies. On the one hand, the angular displacement is more difficult than the linear displacement in the identification process; on the other hand, the error in the moment of inertia caused by the LEDs structure in the orbiter may also result in the disparity observed in the pitching angle as shown in Fig 10b. The trajectory results show that the interstage gap in the AoA = 4.5 deg case is smaller than that at the AoA = 8.3 deg case, which corresponds to the Schlieren results. The orbiter separates from the booster with a slightly higher transverse displacement at AoA = 8.3 deg as shown in Fig 10a. The pitching angle of the orbiter at AoA = 8.3 deg varies at a greater rate than that at AoA = 4.5 deg as shown in Fig 10b. Figure 11 presents the separation process of the TSTO at AoA = 8.3 deg captured by the high-speed camera II. The results directly show that the orbiter separates from the booster successfully and the interstage gap is small. Moreover, the light around the stages in Fig 11 is the self-luminescence effect of hypersonic flow in the shock tunnel.

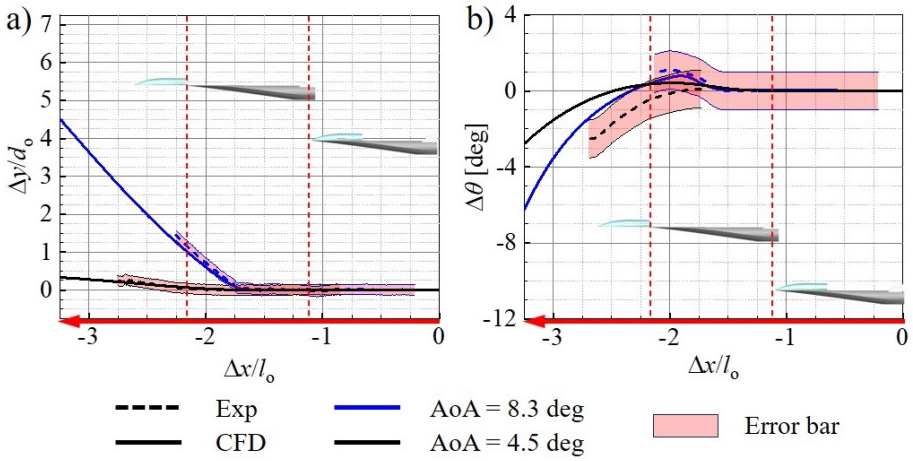

Fig 10. Separation traces results of the LSS test with CFD prediction results.

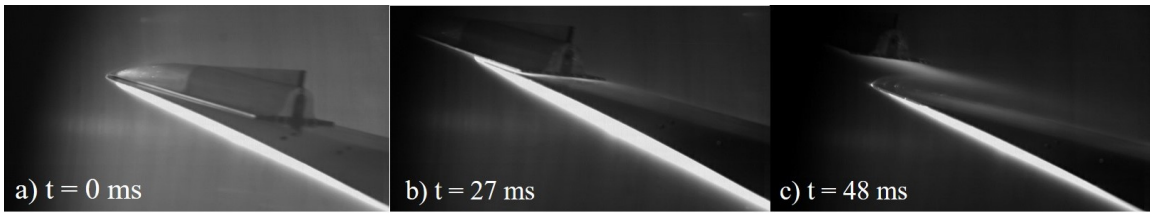

Fig 11. High-speed camera II photos of the LSS test at AoA = 8.3 deg.

5. Conclusion

The aerodynamic interference of LSS is weak. No stage recontact is observed during LSS, and the safety and feasibility of LSS for the parallel-staged TSTO model are demonstrated experimentally, which is important for the success of the future TSTO system. In future work, LSS tests will be conducted under more AoA conditions to further verify the most appropriate condition for the LSS of TSTO. The effects of AoA on LSS characteristics and detailed flowfields should be investigated in combination with numerical simulations.

References

1. Wang, Y., Wang, Y.P., Xue, X.P., Jiang, Z.L.: Numerical investigation on safe stage separation problem of a TSTO model at Mach 7. Chinese Journal of Theoretical and Applied Mechanics. 54, 526-542 (2022)
2. Wang, Y., Wang, Y.P., Jiang, Z.L.: Numerical investigation of aerodynamic separation schemes for two-stage-to-orbit-like two-body system. Aerospace Science and Technology. 131, 107995 (2022)
3. Moelyadi, M.A., Breitsamter, C., Laschka, B.: Stage-separation aerodynamics of two-stage space transport systems Part 2: unsteady simulation. Journal of Spacecraft and Rockets. 45, 1240-1250 (2008)
4. Bordelon, W., Frost, A., Reed, D.: Stage separation wind tunnel tests of a generic TSTO launch vehicle. 21st AIAA Applied Aerodynamics Conference. AIAA 2003-4227, 2003.
5. Wang, Y., Wang, Y.P.: Unsteady interaction and dynamic stability analysis of a two-stage-to-orbit vehicle during transverse stage separation. Acta Astronautica. 216, 488-503 (2024)
6. Wang, Y., Wang, Y.P., Jiang, Z.L.: Unsteady interaction mechanism of transverse stage separation in hypersonic flow for a two-stage-to-orbit vehicle. Physics of Fluids. 35, 056120 (2023)

7. Wang, Y., Wang, Y.P., Wang, C., Jiang, Z.L.: Numerical study of the longitudinal stage separation for parallel-staged two-stage-to-orbit vehicle. Acta Aeronautica et Astronautica Sinica. 44, 127634 (2023)
8. Wang, Y., Wang, Y.P., Wang, C., Jiang, Z.L.: Numerical investigation on a longitudinal-stage-separation of spiked two-stage-to-orbit vehicle. Journal of Spacecraft and Rockets. 60, 215-229 (2023)
9. Jiang, Z. L.: Experiments and development of long-test-duration hypervelocity detonation-driven shock tunnel (LHDst). 52nd Aerospace Sciences Meeting. AIAA-2014-1012, 2014
10. Jiang, Z. L., Chue, RANDY S. M.: Theories and technologies of hypervelocity shock tunnels. Cambridge University Press. 2023
11. Wang, Y., Wang, Y.P., Jiang, Z.L.: Experimental study of longitudinal stage separation of two-body configuration in shock tunnel. AIAA Journal. 60, 6940-6946 (2022)
12. Wang, Y., Wang, Y.P., Jiang, Z.L.: Test technology of longitudinal stage separation for two-stage-to-orbit vehicle in shock tunnel. Acta Aeronautica et Astronautica Sinica. 44, 128126 (2023) (in Chinese)